Chiral Inhibition of Rivaroxaban Derivatives Towards UDP-Glucuronosyltransferase (UGT) Isoforms

ZHUHUA YAO,[1,†] YONG-ZHE LIU,[3,†] AI-LUN MA,[2] SHU-FEN WANG,[3] DAN LU,[5] CUI-MIN HU,[6] YAN-YAN ZHANG,[7] HAINA WANG,[8] LINGYUN HU,[9] JUN DENG,[2,4*] KUN YANG,[3*] AND ZHONG-ZE FANG[3*]

[1]*Department of Cardiology, Tianjin Union Medicine Centre, 300121, Tianjin, People's Republic of China*
[2]*School of Pharmaceutical Science and Technology, Key Laboratory for Modern Drug Delivery & High-Efficiency, Tianjin University, Tianjin, People's Republic of China*
[3]*Department of Toxicology, School of Public Health, Tianjin Medical University, Tianjin, People's Republic of China*
[4]*Collaborative Innovation Center of Chemical Science and Engineering, Tianjin University, Tianjin, People's Republic of China*
[5]*Department of Immunology, Tianjin Key Laboratory of Cellular and Molecular Immunology, Tianjin Medical University, Tianjin, People's Republic of China*
[6]*Tianjin Life Science Research Center, Department of Microbiology, School of Basic Medical Sciences, Tianjin Medical University, Tianjin, People's Republic of China*
[7]*Joint Center for Translational Medicine, Dalian Institute of Chemical Physics, Chinese Academy of Sciences and First Affiliated Hospital of Liaoning Medical University, Dalian, People's Republic of China*
[8]*College of Pharmaceutical Sciences, Shandong University, Jinan, People's Republic of China*
[9]*Shandong Cancer Hospital and Institute, Shandong, People's Republic of China*

ABSTRACT Rivaroxaban is an oral direct factor Xa (FXa) inhibitor clinically used to prevent and treat thromboembolic disorders. Drug–drug interaction (DDI) exist for rivaroxaban and the inhibitors of CYP3A4/5. This study aims to investigate the inhibition of rivaroxaban and its derivatives with a chiral center towards UDP-glucuronosyltransferases (UGTs). Chemical synthesis was performed to obtain rivaroxaban derivatives with different chiral centers. UGTs supersomes-catalyzed 4-methylumbelliferone (4-MU) glucuronidation was employed to evaluate the inhibition potential towards various UGT isoforms. A significant influence of rivaroxaban derivatives towards UGT1A3 was observed. Chiral centers produce different effects towards the effect of four pairs of rivaroxaban derivatives towards UGT1A3 activity, with stronger inhibition potential of S1 than R1, but stronger inhibition capability of R2, R3, R4 than S2, S3, and S4. Competitive inhibition of R3 and R4 towards UGT1A3 was demonstrated by Dixon and Lineweaver-Burk plots. In conclusion, the significant influence of rivaroxaban derivatives towards UGT1A3's activity was demonstrated in the present study. The chirality centers highly affected the inhibition behavior of rivaroxaban derivatives towards UGT1A3. *Chirality 27:936–943, 2015.*

KEY WORDS: rivaroxaban; UDP-glucuronosyltransferases (UGTs); drug-drug interaction; chirality

Rivaroxaban is an oral direct factor Xa (FXa) inhibitor, and has been clinically used to prevent and treat thromboembolic disorders.[1] Based on the structural basis of rivaroxaban, many efficient derivatives were prepared to investigate the structure–activity relationship for antithrombotic therapies.[2] Rivaroxaban has one (S)-type chiral center, and different types of chiral centers have been introduced into the structures of rivaroxaban derivatives. The (S)-enantiomer has stronger therapeutic efficacy, and the (R)-enantiomer and its derivatives have not served as drugs, but might be useful in the new therapeutic utilization of rivaroxaban.

Rivaroxaban can be rapidly absorbed after oral administration. Cytochrome P450 (CYP)-catalyzed oxidation and CYP-independent hydrolytic reaction have been demonstrated to be the major metabolic pathway of rivaroxaban.[3] The major involved CYP isoforms contain CYP3A4/5 and CYP2J2.[4] Drug–drug interaction was highly speculated to be involved between rivaroxaban and the strong inhibitors of CYP3A4/5.[4]

Human UDP-glucuronosyltransferases (UGTs) are important phase II drug-metabolizing enzymes involved in the glucuronidation of drugs or their phase I metabolites.[5] The UGTs-catalyzed glucuronidation reaction plays a key role in detoxification of endogenous and exogenous substances.[6] For example, intestinal UGT1A1 protects irinotecan-induced diarrhea through catalyzing the glucuronidation of SN-38, which is the active substance of irinotecan.[7] The inhibition of the SN-38 glucuronidation process by xenobiotics can result in the elevation of the toxicity intensity of irinotecan.[8–10] The inhibition towards the UGTs-catalyzed reaction can also disrupt the metabolism of endogenous substances, such as the influence of indinavir and sorafenib towards the metabolism of bilirubin.[11] The inhibition of rivaroxaban and its derivatives towards UGTs' activity was investigated in the present study.

Drugs with different chiral centers will exert varied pharmacokinetic properties. For example, terazosin enantiomers exhibited different pharmacokinetic behaviors in healthy Chinese male subjects.[12] A completely different metabolic pathway was elucidated for praziquantel (PZQ), which is a

*Correspondence to: Jun Deng, School of Pharmaceutical Science and Technology, Key Laboratory for Modern Drug Delivery & High-Efficiency, Tianjin University, Tianjin, 300072 People's Republic of China. E-mail: jdeng@tju.edu.cn
Kun Yang or Zhong-Ze Fang, Department of Toxicology, School of Public Health, Tianjin Medical University, Tianjin, China. E-mail: yangkun@tijmu.edu.cn or fangzhongze@tijmu.edu.cn
†These two authors equally contributed to this work.
Received for publication 17 April 2015; Accepted 19 July 2015
DOI: 10.1002/chir.22505
Published online 1 October 2015 in Wiley Online Library (wileyonlinelibrary.com).

prevalent drug to treat schistosomiasis.[10] Drug metabolism-related drug–drug interaction can also be affected by chiral properties. For example, the experiment performed by Sun et al. showed the strong stereoselective interaction between tetrahydropalmatine enantiomers and cytochrome P450 (CYP) isoforms.[13] Our recent work also demonstrated that (S)-carprofen exhibited stronger inhibition than (R)-carprofen towards the activity of phase II DME UDP-glucuronosyltransferase (UGT) 2B7.[14]

The aim of this study was to investigate the inhibition of rivaroxaban and its derivatives towards UGT isoforms. The compounds with different chiral centers were synthesized and the inhibition potential was determined using recombinant UGTs-catalyzed 4-methylumbelliferone (4-MU) glucuronidation reaction.

MATERIALS AND METHODS

Materials

4-Methylumbelliferone (4-MU), 4-methylumbelliferone-β-D-glucuronide (4-MUG), Tris-HCl, 7-hydroxycoumarin, and uridine-5′-diphosphoglucuronic acid trisodium salt (UDPGA) were purchased from Sigma-Aldrich (St. Louis, MO). Recombinant human UGT isoforms (UGT1A1, UGT1A3, UGT1A6, UGT1A7, UGT1A8, UGT1A9, UGT1A10, UGT2B7) expressed in baculovirus-infected insect cells were obtained from BD Gentest (Woburn, MA). All other reagents were of high-performance liquid chromatography (HPLC) grade or of the highest grade commercially available.

Chemical Synthesis of Rivaroxaban and Its Derivatives

All synthesis reactions were performed in flame-dried glassware under a nitrogen atmosphere. Solvents were distilled prior to use. Reagents were purchased from J&K Scientific (China), Beijing Ouhe (China), Aldrich (Milwaukee, WI), Acros (Somerville, NJ), Alfa Aesar (Ward Hill, MA), or TCI (Portland, OR) unless otherwise noted. Chromatographic separations were performed using Kangbino 48-75 Å SiO_2. ^1H and ^{13}C NMR spectra were obtained on 400 MHz Bruker Avance (Billerica, MA) spectrometers using $CDCl_3$ with tetramethylsilane (TMS) or residual solvent as standard unless otherwise noted. Melting points were determined using a Laboratory Devices MEL-TEMP and were uncorrected/calibrated. Thin-layer chromatography (TLC) analysis was performed using Kangbino glass-backed plates (60 Å, 250 μm) and visualized using UV and $KMnO_4$ stains. Low-resolution mass spectra were obtained using an Agilent (Palo Alto, CA) 1100 series LS/MSD. High-resolution mass spectra were obtained using a Q-TOF micro (Bruker) spectrometer. Compounds 4-{4-[(5R)-5-(Aminomethyl)-2-oxo-1,3-oxazolidin-3-yl]phenyl}morpholin -3-one and 4-{4-[(5S)-5-(Aminomethyl)-2-oxo-1,3-oxazolidin-3-yl]phenyl}morpholin-3-one were synthesized according to the literature procedure.[2]

5-Chloro-N-({(5S)-2-oxo-3-[4-(3-oxomorpholin-4-yl)-phenyl]-1,3-oxazolidin-5-yl}methyl)-thiophene-2-carboxamide (S1). To a solution of 5-chlorothiophene-2-carboxylic acid (13.3 mg, 0.082 mmol) in CH_2Cl_2 (2.0 mL) was added DCC (28 mg, 0.136 mmol) at room temperature. The resulting mixture was stirred for 2 h. After which 4-{4-[(5S)-5-(aminomethyl)-2-oxo-1,3-oxazolidin-3-yl]phenyl}morpholin-3-one (14.5 mg, 0.05 mmol) was added. Then the mixture was stirred for 6 h at room temperature. The mixture was then quenched with H_2O and extracted with CH_2Cl_2 (5 mL × 3). The combined organic phase was dried over Na_2SO_4 and concentrated under reduced pressure. The resulting crude product was purified via flash column chromatography (SiO_2; isocratic eluent: 3% MeOH in CH_2Cl_2) to provide S1 as a white solid in 36% yield (8.0 mg), yield: 36%; mp: 233–235°C; R_f = 0.71 (MeOH:CH_2Cl_2 = 1:10); [α]D23 = –33.75 [c 0.1 MeOH]; ^1H NMR (400 MHz, $CDCl_3$) δ 3.63–3.84 (m, 5H), 4.02–4.06 (m, 3H), 4.33 (s, 2H), 4.81 (br, 1H), 6.85–6.86 (d, J = 4.0 Hz, 1H), 7.04 (t, J = 5.96 Hz, 1H), 7.33 (t, J = 6.84 Hz, 3H), 7.52–7.54 (d, J = 8.92 Hz, 2H); 13C NMR (100 MHz, $CDCl_3$) δ 42.4, 47.6, 49.7, 64.1, 68.5, 71.8, 119.1, 126.3, 127.1, 127.9, 136.0, 136.5, 136.6, 137.2, 154.4, 161.7, 166.9; mass spectrum (ESI): m/e (% relative intensity) 436.8 (100) $(M+H)^+$; HRMS (ESI): m/z calcd for C19H18O5N3SCl $(M+H)^+$ 436.0734.

N-({(5S)-2-oxo-3-[4-(3-oxomorpholin-4-yl)-phenyl]-1,3-oxazolidin-5-yl}methyl)-thiophene-2-carboxamide (S2). Compound S2 was synthesized according to the procedure described for S1, yield: 48%; mp: 200–203°C; Rf = 0.70 (MeOH:CH_2Cl_2 = 1:10); [α]D23 = –44.62 [c 0.1 MeOH]; 1H NMR (400 MHz, $CDCl_3$) δ 3.70–3.77 (m, 3H), 3.83–3.89 (m, 2H), 4.02–4.10 (m, 3H), 4.33 (s, 2H), 4.85 (br, 1H), 6.77 (t, J = 5.98 Hz, 1H), 7.07 (t, J = 4.36 Hz, 1H), 7.31–7.33 (d, J = 8.88 Hz, 2H), 7.49–7.51 (dd, J = 0.78, 4.96 Hz, 1H), 7.54–7.56 (d, J = 8.92 Hz); 13C NMR (100 MHz, CDCl3) δ 42.3, 47.7, 49.6, 64.1, 68.5, 71.9, 119.1, 126.2, 127.8, 128.7, 130.8, 136.6, 137.2, 154.3, 162.6, 166.8; mass spectrum (ESI): m/e (% relative intensity) 423.8 (100) $(M+Na)^+$; HRMS (ESI): m/z calcd for C19H19O5N3S (M+Na)+ 424.0943.

5-Bromo-N-({(5S)-2-oxo-3-[4-(3-oxomorpholin-4-yl)-phenyl]-1,3-oxazolidin-5-yl}methyl)-thiophene-2-carboxamide (S3). Compound S3 was synthesized according to the procedure described for S1, yield: 37%; mp: 205–208°C; Rf = 0.70 (MeOH:CH_2Cl_2 = 1:10); [α]D23 = –20.00 [c 0.1 MeOH]; 1H NMR (400 MHz, $CDCl_3$) δ 3.65–3.85 (m, 5H), 4.02–4.05 (m, 3H), 4.33 (s, 2H), 4.82 (br, 1H), 6.96 (t, J = 5.86 Hz, 1H), 7.00–7.01 (d, J = 3.96 Hz, 1H), 7.30 (t, J = 6.88 Hz, 3H), 7.52–7.55 (d, J = 8.88 Hz, 2H), 7.54–7.56 (d, J = 8.92 Hz); 13C NMR (100 MHz, $CDCl_3$) δ 42.4, 47.6, 49.7, 64.1, 68.5, 71.8, 119.1, 126.3, 128.7, 130.8, 136.6, 137.3, 154.3, 161.6, 166.9; mass spectrum (ESI): m/e (% relative intensity) 503.4 (100) $(M+Na)^+$; HRMS (ESI): m/z calcd for C19H18O5N3SBr $(M+Na)^+$ 502.0048.

6-Chloro-N-({(5S)-2-oxo-3-[4-(3-oxomorpholin-4-yl)phenyl]-1,3-oxazolidin-5-yl}methyl)pyridine-2-carboxamide (S4). Compound S4 was synthesized according to the procedure described for S1, yield: 27%; mp: 117–120°C; Rf = 0.70 (MeOH:CH_2Cl_2 = 1:10); [α]D23 = –72.69 [c 0.1 MeOH]; 1H NMR (400 MHz, $CDCl_3$) δ 3.72–3.96 (m, 5H), 4.03 (t, J = 4.96 Hz, 2H), 4.12 (t, J = 8.9 Hz, 1H) 4.33 (s, 2H), 4.89 (br, 1H), 7.31–7.33 (d, J = 8.8 Hz, 2H), 7.47–7.49 (d, J = 7.92 Hz, 1H), 7.55–7.58 (d, J = 8.84 Hz, 2H), 7.82 (t, J = 7.76 Hz, 1H), 8.08–8.10 (d, J = 7.52 Hz), 8.29 (t, J = 6.2 Hz); 13C NMR (100 MHz, $CDCl_3$) δ 42.2, 47.8, 49.6, 53.4, 64.1, 68.5, 71.7, 119.0, 121.1, 126.1, 127.5, 136.7, 137.2, 140.0, 149.4, 150.3, 154.2, 163.9, 166.8; mass spectrum (ESI): m/e (% relative intensity) 452.7 (100) $(M+Na)^+$; HRMS (ESI): m/z calcd for C20H19O5N3SCl $(M+Na)^+$ 453.0942.

5-Chloro-N-({(5R)-2-oxo-3-[4-(3-oxomorpholin-4-yl)-phenyl]-1,3-oxazolidin-5-yl}methyl)-thiophene-2-carboxamide (R1). Compound R1 was synthesized according to the procedure described for S1, yield: 34%; mp: 233–235°C; Rf = 0.71 (MeOH:CH_2Cl_2 = 1:10); [α]D23 = 76.67 [c 0.1 MeOH]; 1H NMR (400 MHz, $CDCl_3$) δ 3.63–3.84 (m, 5H), 4.02–4.06 (m, 3H), 4.33 (s, 2H), 4.81 (br, 1H), 6.85–6.86 (d, J = 4.0 Hz, 1H), 7.04 (t, J = 5.96 Hz, 1H), 7.33 (t, J = 6.84 Hz, 3H), 7.52–7.54 (d, J = 8.92 Hz, 2H); 13C NMR (100 MHz, $CDCl_3$) δ 42.4, 47.6, 49.7, 64.1, 68.5, 71.8, 119.1, 126.3, 127.1, 127.9, 136.0, 136.5, 136.6, 137.2, 154.4, 161.7, 166.9; mass spectrum (ESI): m/e (% relative intensity) 436.8 (100) (M+H)+; HRMS (ESI): m/z calcd for C19H18O5N3SCl (M+H)+ 436.0734.

N-({(5R)-2-oxo-3-[4-(3-oxomorpholin-4-yl)-phenyl]-1,3-oxazolidin-5-yl}methyl)-thiophene-2-carboxamide (R2). Compound R2 was synthesized according to the procedure described for S1, yield: 57%; mp: 200–203°C; Rf = 0.70 (MeOH:CH_2Cl_2 = 1:10); [α]D23 = –44.62 [c 0.1 MeOH]; 1H NMR (400 MHz, CDCl3) δ 3.70–3.77 (m, 3H), 3.83–3.89 (m, 2H), 4.02–4.10 (m, 3H), 4.33 (s, 2H), 4.85 (br, 1H), 6.77 (t, J = 5.98 Hz, 1H), 7.07 (t, J = 4.36 Hz, 1H), 7.31–7.33 (d, J = 8.88 Hz, 2H), 7.49–7.51 (dd, J = 0.78, 4.96 Hz, 1H), 7.54–7.56 (d, J = 8.92 Hz); 13C NMR (100 MHz, CDCl3) δ 42.3, 47.7, 49.6, 64.1, 68.5, 71.9, 119.1, 126.2, 127.8, 128.7, 130.8, 136.6, 137.2, 154.3, 162.6, 166.8; mass spectrum (ESI): m/e (% relative intensity) 423.8 (100) $(M+Na)^+$; HRMS (ESI): m/z calcd for C19H19O5N3S $(M+Na)^+$ 424.0943.

5-Bromo-N-({(5R)-2-oxo-3-[4-(3-oxomorpholin-4-yl)-phenyl]-1,3-oxazolidin-5-yl}methyl)-thiophene-2-carboxamide (R3). Compound R3 was synthesized according to the procedure described for S1,: yield: 42%; mp: 205–208°C; Rf = 0.70 (MeOH:CH_2Cl_2 = 1:10);

[α]D23 = –20.00 [c 0.1 MeOH]; 1H NMR (400 MHz, $CDCl_3$) δ 3.65–3.85 (m, 5H), 4.02–4.05 (m, 3H), 4.33 (s, 2H), 4.82 (br, 1H), 6.96 (t, J = 5.86 Hz, 1H), 7.00–7.01 (d, J = 3.96 Hz, 1H), 7.30 (t, J = 6.88 Hz, 3H), 7.52–7.55 (d, J = 8.88 Hz, 2H), 7.54–7.56 (d, J = 8.92 Hz); 13C NMR (100 MHz, $CDCl_3$) δ 42.4, 47.6, 49.7, 64.1, 68.5, 71.8, 119.1, 126.3, 128.7, 130.8, 136.6, 137.3, 154.3, 161.6, 166.9; mass spectrum (ESI): m/e (% relative intensity) 503.4 (100) $(M+Na)^+$; HRMS (ESI): m/z calcd for C19H18O5N3SBr $(M+Na)^+$ 502.0048.

6-Chloro-N-({(5R)-2-oxo-3-[4-(3-oxomorpholin-4-yl)phenyl]-1,3-oxazolidin-5-yl}methyl)pyridine-2-carboxamide (R4). Compound R4 was synthesized according to the procedure described for S1, yield: 26%; mp: 117–120°C; Rf = 0.70 (MeOH:CH2Cl2 = 1:10); [α]D23 = –72.69 [c 0.1 MeOH]; 1H NMR (400 MHz, CDCl3) δ 3.72–3.96 (m, 5H), 4.03 (t, J = 4.96 Hz, 2H), 4.12 (t, J = 8.9 Hz, 1H) 4.33 (s, 2H), 4.89 (br, 1H), 7.31–7.33 (d, J = 8.8 Hz, 2H), 7.47–7.49 (d, J = 7.92 Hz, 1H), 7.55–7.58 (d, J = 8.84 Hz, 2H), 7.82 (t, J = 7.76 Hz, 1H), 8.08–8.10 (d, J = 7.52 Hz), 8.29 (t, J = 6.2 Hz); 13C NMR (100 MHz, CDCl3) δ 42.2, 47.8, 49.6, 53.4, 64.1, 68.5, 71.7, 119.0, 121.1, 126.1, 127.5, 136.7, 137.2, 140.0, 149.4, 150.3, 154.2, 163.9, 166.8; mass spectrum (ESI): m/e (% relative intensity) 452.7 (100) $(M+Na)^+$; HRMS (ESI): m/z calcd for C20H19O5N3SCl $(M+Na)^+$ 453.0942.

In Vitro Incubation Mixture to Determine the Inhibitory Capability

The in vitro incubation system to evaluate the inhibition of UGTs' activity by compounds has been described in the previous literature.[14,15] In brief, the incubation system (total volume = 200 μL) contained recombinant human UGT isoforms, 5 mM UDPGA, 5 mM $MgCl_2$, 50 mM Tris-HCl (pH = 7.4), and 4-MU in the absence or presence of different concentrations of various rivaroxaban or its derivatives. The incubation time used and protein concentration were previously determined to ensure the reaction rate within the linear range. The incubation reaction was initiated through addition of UDPGA to the mixture after a 5-min preincubation at 37°C. The reactions were quenched by adding 100 μL acetonitrile with 7-hydroxycoumarin (100 μM) as internal standard. The mixture was centrifuged at 20,000*g* for 10 min, and an aliquot of supernatant was transferred to an autoinjector vial for HPLC analysis. The HPLC system (Shimadzu, Kyoto, Japan) contained an SCL-10A system controller, two LC-10AT pumps, an SIL-10A autoinjector, and an SPD-10AVP UV detector. Chromatographic separation was carried out using a C18 column (4.6 × 200 mm, 5 μm, Kromasil) at a flow rate of 1 mL/min and UV detector at 316 nm. The mobile phase consisted of acetonitrile (A) and H_2O containing 0.5% (v/v) formic acid (B). The following gradient condition was used: 0–15 min, 95–40% B; 15–20 min, 10% B; 20–30 min, 95% B. The calculation curve was generated by peak area ratio (4-MUG/internal standard) over the concentration range of 4-MUG 0.1–100 mM. The curve was linear over this concentration range, with an r^2 value >0.99. The limits of detection and quantification were determined at signal-to-noise ratios of 3 and 10, respectively. The accuracy and precision for each concentration were more than 95%.

Molecular Docking

The 3D structure of the UGT1A3 enzyme is still unknown. Thus, we developed a 3D structure for the UGT1A3 enzyme. The homology modeling method has been applied to the building of this 3D model. The amino acid sequence of the UGT1A3 enzyme in the FASTA format was retrieved from the NCBI database (Accession number: NP061966), which was used for homology modeling of the 3D structure of the UGT1A3 enzyme. The templates for homology modeling of the UGT1A3 structure were included the crystal structures of oleandomycin glycosyltransferase (PDB code: 2iya), flavonoid 3-O glycosyltransferase (PDB code: 2c1x), and hydroquinone glucosyltransferase (PDB code: 2vce). The Modeller 9v14 program was used for predicting the 3D model of the UGT1A3 enzyme according to the known crystal structures of homologous proteins. The best model can be selected based on the lowest value of the Modeller objective function and DOPE (discrete optimization protein energy) score build by the Modeller program. PROCHECK was used to determine the stereochemical quality of the prediction model, and check the rationality of the predicted enzyme structure.

For better understanding the molecular interactions between ligand and protein, the docking between flexible small molecule and rigid protein was performed using Autodock v. 4.2. Eight compounds (S1, R1, S2, R2, S3, R3, S4, R4) were docked into the UGT1A3 enzyme. The nonpolar hydrogen atoms of the UGT1A3 enzyme were merged, and Kollman charges were then added to the protein structure using the AutoDockTool. Gasteiger partial charges were assigned to the eight inhibitors. The grid points for Autogrid calculations were set to 100*100*100, which was large enough to cover the entire ligand-binding site and accommodate ligands to move freely. The grid point spacing for grid-box was 0.375 Å. The Lamarckian genetic algorithm (LGA) was used for protein-fixed ligand-flexible docking calculations. Fifty search attempts (ga_run parameter) were performed for each ligand. Other docking parameters were set to the software's default values. After the docking search was completed, the best conformation was chosen with the lowest docked energy. The interactions between inhibitors and the UGT1A3 enzyme including hydrogen bonds and hydrophobic interactions were analyzed.

Inhibition Kinetic Determination

For some representative compounds R3 and R4, the inhibition kinetic behaviors (including kinetic type and parameters) were determined. The reaction velocity was determined at different concentrations of substrates and inhibitors, and the incubation time is the same as that in the initial screening study. The two most common plot methods (Dixon and Lineweaver-Burk plots) to determine the inhibition type were employed in the present study. The inhibition parameters (K_i) were calculated through correlating the slopes from the Lineweaver-Burk plots versus the concentrations of inhibitors.

RESULTS

Inhibition Profiles of Rivaroxaban Derivatives Towards Various UGT Isoforms

The inhibition potential of rivaroxaban derivatives towards various UGT isoforms was investigated at 100 μM. As shown in Figure 1, 100 μM of rivaroxaban derivatives weakly inhibited the activity of UGT1A1, UGT1A6, UGT1A8, UGT1A9, UGT1A10, and UGT2B7, with less than 75% inhibition towards all these UGT isoenzymes. For UGT1A3 inhibition by rivaroxaban derivatives, the activity of UGT1A3 was inhibited 73.9%, 44.5%, 49.3%, 74.7%, 43.9%, 78.5%, 45.3%, 83.9% by S1, R1, S2, R2, S3, R3, S4, and R4, respectively. S4 inhibited more than 75% activity of UGT1A7-catalyzed 4-MU glucuronidation. Other rivaroxaban derivatives exhibited weak inhibition capability towards UGT1A7-catalyzed 4-MU glucuronidation, with the activity of UGT1A7 inhibited by less than 75%. The chiral properties exhibited influence on the inhibition capability towards UGT1A1 and UGT1A3-catalyzed 4-MU glucuronidation. R2 and R4 exhibited stronger inhibition potential towards the activity of UGT1A1 than S2 and S4 ($P < 0.05$). S1 exerted stronger inhibition towards UGT1A3 than R1 ($P < 0.01$). In contrast, R2, R3, and R4 showed stronger inhibition potential than S1, S2, and S3 ($P < 0.01$). Furthermore, concentration-dependent inhibition behavior was determined (Fig. 2). The results showed that S1 exhibited stronger inhibition potential than R1 towards UGT1A3 at tested concentrations. In contrast, R2, R3, and R4 exerted stronger inhibition ability than S2, S3, and S4 in a concentration-dependent manner.

Molecular Docking to Understand the Interaction Between Rivaroxaban Derivatives and UGT1A3

Eight inhibitors were docked into the cavity of UGT1A3 by molecular docking method (Fig. 3A), which explored the interactions between ligand and protein. It is a big task to

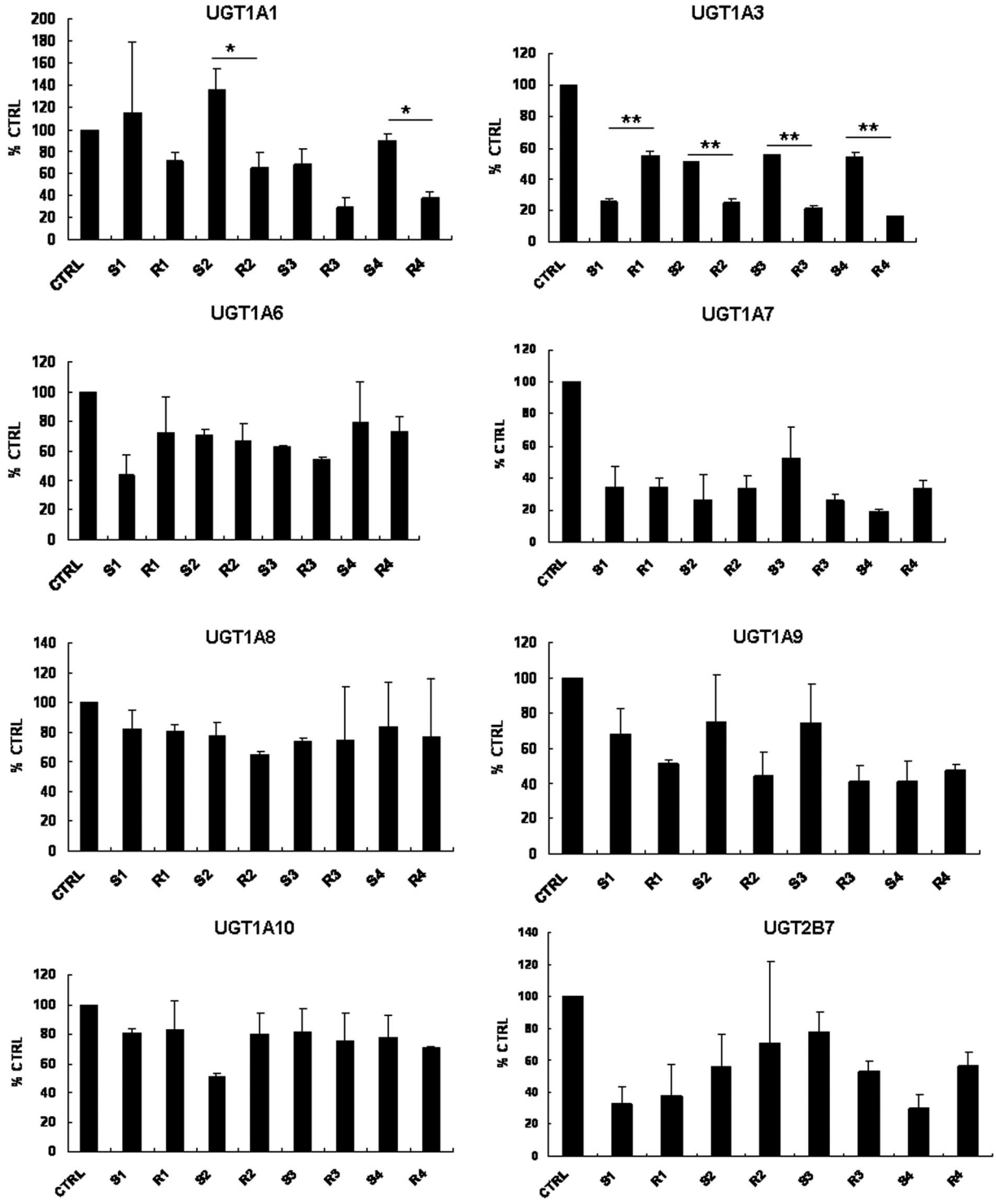

Fig. 1. Screening of inhibitory capability of rivaroxaban derivatives towards recombinant UGT isoforms-catalyzed 4-MU glucuronidation. The incubation system (total volume = 200 μL) contained recombinant human UGT isoforms, 5 mM UDPGA, 5 mM $MgCl_2$, 50 mM Tris-HCl (pH = 7.4), 4-MU, and 100 μM of rivaroxaban derivatives. The residual activity (% control) = the activity of UGTs-catalyzed 4-MU glucuronidation at 100 μM of rivaroxaban derivatives / the activity of UGTs-catalyzed 4-MU glucuronidation at 0 μM of rivaroxaban derivatives *100%.

recognize the ligand binding domain of UGT1A3, and the molecular docking method was used to generate the active pocket of UGT1A3. The active site of UGT1A3 enzyme for binding with S1, R1, S2, R2, S3, R3, S4, and R4 is composed of residues Ser39, His40, Leu42, Leu77, Arg112, Ser113, Met116, Leu117, Met120, Val154, Arg174, Asn175, Cys224, His225, Phe239, Arg258, Asn283, Arg284, Lys285, Ser307, Leu308, Gly309, Ser310, Val312, Ser313, Arg337, Trp355, Leu356, Pro357, Gln358, Asn359, His373, Ala374, Gly375, Ser376, His377, Gly378, Gln381, Phe395, Gly396, Asp397, Gln398, and Asn401, which is shown in Figure 3B. In the active pocket of UGT1A3, eight inhibitors made hydrogen bonds to UGT1A3 enzyme, which are shown in Figure 4. Ligand S1 formed a hydrogen bond with residues Ser39, Ser376, His377, Gly378, and Asp397 in the active pocket of the UGT1A3 enzyme; however, ligand R1 just formed four

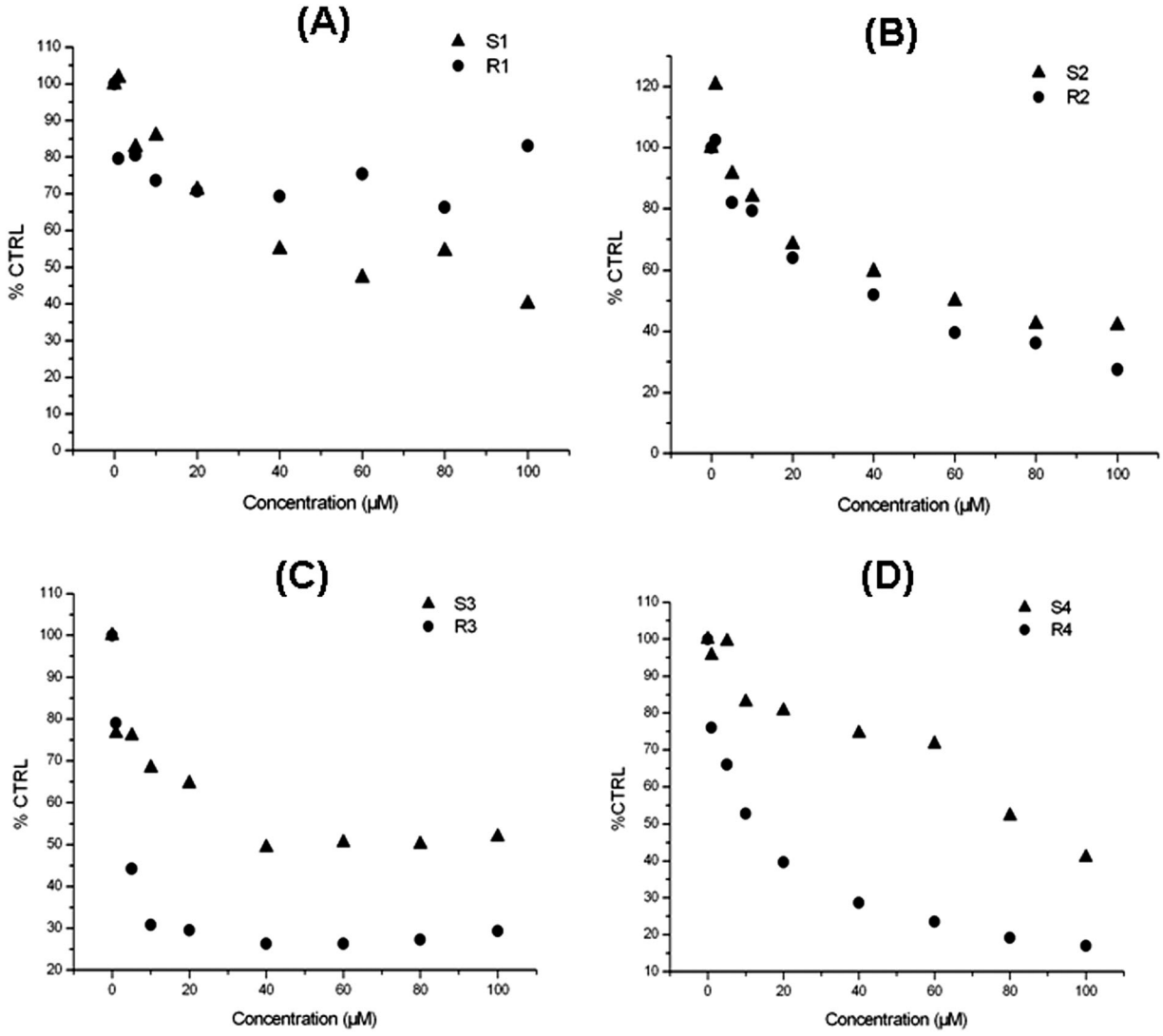

Fig. 2. Concentration-dependent inhibition of rivaroxaban derivatives towards recombinant UGT1A3-catalyzed 4-MU glucuronidation. Each data point represents the mean value of duplicate experiments.

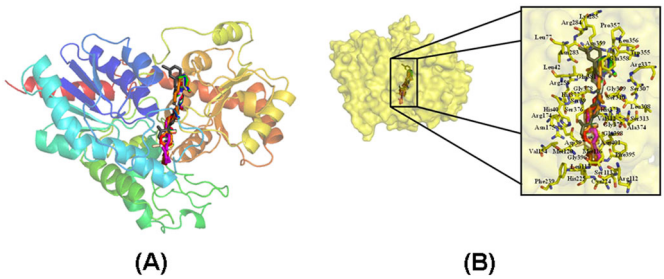

Fig. 3. The binding of eight rivaroxaban derivatives towards the activity cavity of UGT1A3. (A) Far view map of the binding of rivaroxaban derivatives towards the activity cavity of UGT1A3; (B) The active pocket of UGT1A3 enzyme binding with inhibitors S1 (red), R1 (green), S2 (magenta), R2 (cyan), S3 (orange), R3 (blue), S4 (gray), and R4 (wheat).

hydrogen bonds, involved in residues Asn175, Ser310, Gln358, and Gln398 in UGT1A3. Ligand S2 made hydrogen bonds with the residues Ser39, Ser376, His377, and Gly378 of UGT1A3, whereas its chiral compound R2 formed different hydrogen bonds. Ligand R2 formed hydrogen bonds with residues Asn175, Ser310, and Gln358 in the active pocket of the UGT1A3 enzyme. Ligand S3 made hydrogen bonds to residue Ser310, Ser376, His377, and Asp397, and its chiral compound R3 formed hydrogen bonds with residues Asn175, Ser310, and Gln358 in the UGT1A3 enzyme. Ligand S4 made hydrogen bonds to residues Asn175 and Glu381, and its chiral compound R4 formed hydrogen bonds with residues Asn175, Ser310, and Gln358 in UGT1A3. The hydrophobic contacts between the eight inhibitors and UGT1A3 appeared in the active pocket of enzyme (Fig. 5). Ligand S1 formed hydrophobic contacts with residues Ser39, Leu117, His225, Gly309, Trp355, Gln358, His373, Gly375, Ser376, His377, Gly378, Glu381, Phe395, and Gly396. Ligand R1 formed analogous hydrophobic contacts with residues Ser39, Gly309, Trp355, Leu356, Gln358, His373, Gly375, His377, Phe395, Gly396, and Gln398. The hydrophobic contacts formed by UGT1A3-S2 contain residues Ser39, Leu42, Leu117, Asn175, Gly309, Gln358, His373, Gly375, His377, Gly378, Phe395, and Gly396. Ligand R2 formed hydrophobic contacts with residues Ser39, Gly309, Trp355, Leu356, Gln358, His373, Gly375, His377, Gly378, Gly396, and Gln398. Ligand S3 made hydrophobic contacts to residues Ser39, Leu42, Leu117, His225, Gly309, Ser310, Trp355, His373, Gly375, Ser376, His377, Phe395, and Gly396. Ligand

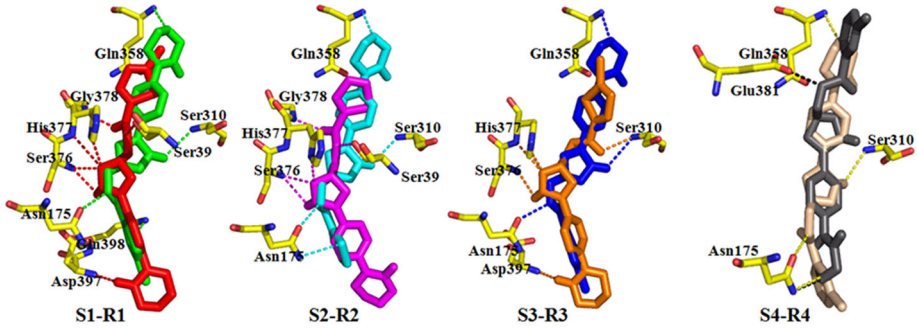

Fig. 4. The UGT1A3 enzyme in complex with S1, R1, S2, R2, S3, R3, S4, and R4, and hydrogen bond is shown by line.

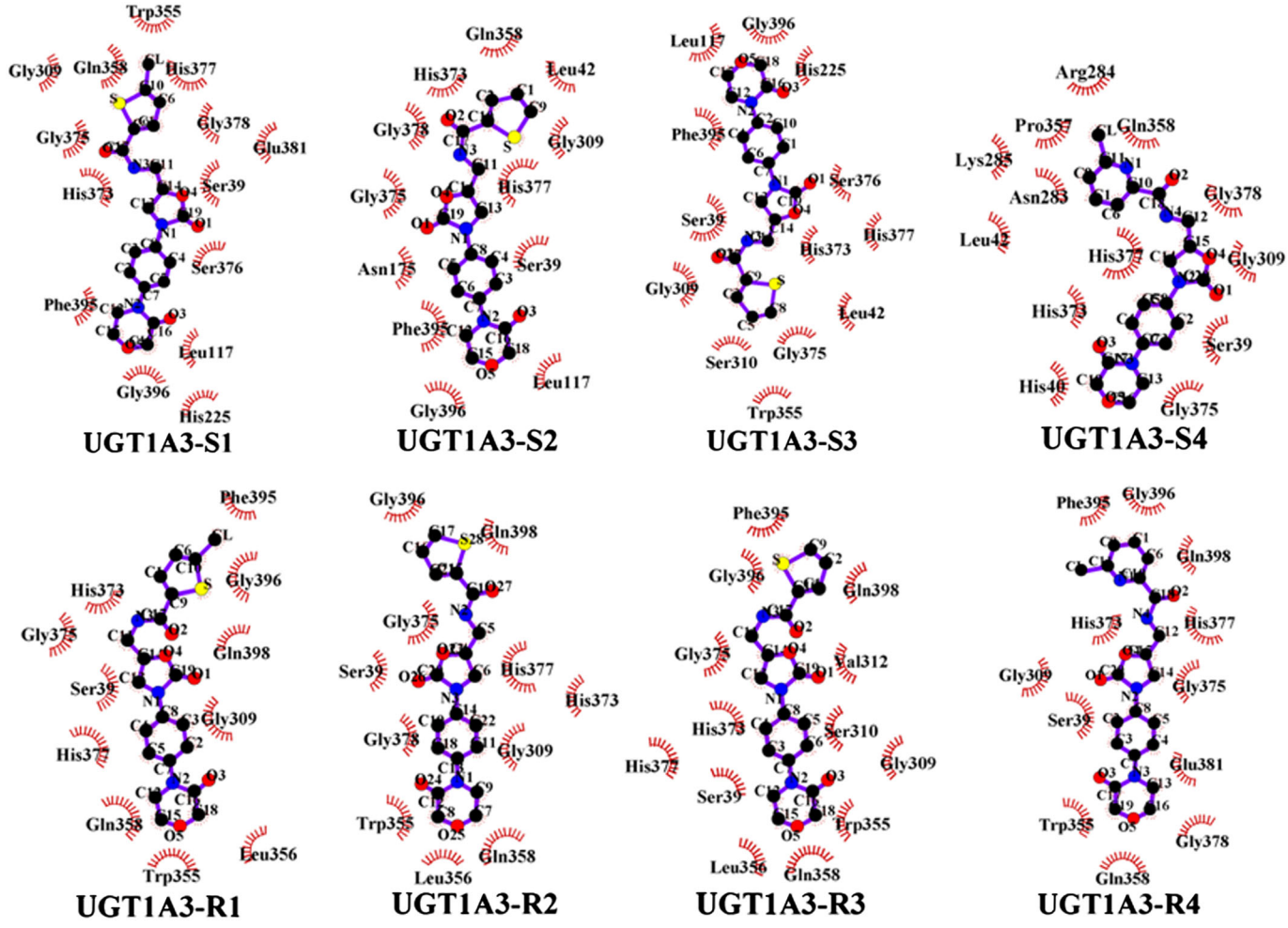

Fig. 5. The hydrophobic contacts between UGT1A3 and S1, R1, S2, R2, S3, R3, S4, and R4. The protein and inhibitors are analysis by LigPlot.

R3 formed hydrophobic contacts with residues Ser39, Gly309, Ser310, Val312, Trp355, Leu356, Gln358, His373, Gly375, His377, Phe395, Gly396, and Gln398. The hydrophobic contacts formed by the interaction of UGT1A3-S4 were involved in residues Ser39, His40, Leu42, Asn283, Arg284, Lys285, Gly309, Pro357, Gln358, His373, Gly375, His377, and Gly378. Ligand R4 made hydrophobic contacts to residues Ser39, Gly309, Trp355, Gln358, His373, Gly375, His377, Gly378, Glu381, Phe395, Gly396, and Gln398.

The top rank in the 50 conformations were obtained from the molecular docking search for results analysis. The eight inhibitors made analogical bind to the UGT1A3 enzyme. We calculated the binding free energy values for the eight inhibitors binding into the UGT1A3 enzyme, the binding free energy value for S1, R1, S2, R2, S3, R3, S4, R4 were –10.61, –10.20, –9.62, –9.90, –9.65, –10.65, –9.28, and –10.74 (Table 1), respectively, which is in accordance with the experimental result that the rank of the inhibition activity for the eight inhibitors were S1>R1, S2<R2, S3<R3, and S4<R4.

Inhibitory Kinetic Type and Parameters of Represent Rivaroxaban Derivatives Towards UGT1A3

R3 and R4 were selected as representative compounds to determine their inhibition kinetics towards UGT1A3-

TABLE 1. Docking results of S1, S2, S3, S4, R1, R2, R3, and R4 with UGT1A3 enzyme

Inhibitor	Intermolecular energy (kcal/mol)	Internal energy (kcal/mol)	Torsional free energy (kcal/mol)	Unbound system's energy (kcal/mol)	Binding free energy (kcal/mol)
S1	−11.80	−0.96	1.19	−0.96	−10.61
S2	−10.81	−0.84	1.19	−0.84	−9.62
S3	−10.84	−1.14	1.19	−1.14	−9.65
S4	−11.07	−0.92	1.19	−0.92	−9.87
R1	−11.69	−0.96	1.49	−0.96	−10.20
R2	−11.09	−1.08	1.19	−1.08	−9.90
R3	−11.84	−0.98	1.19	−0.98	−10.65
R4	−11.94	−0.85	1.19	−0.85	−10.74

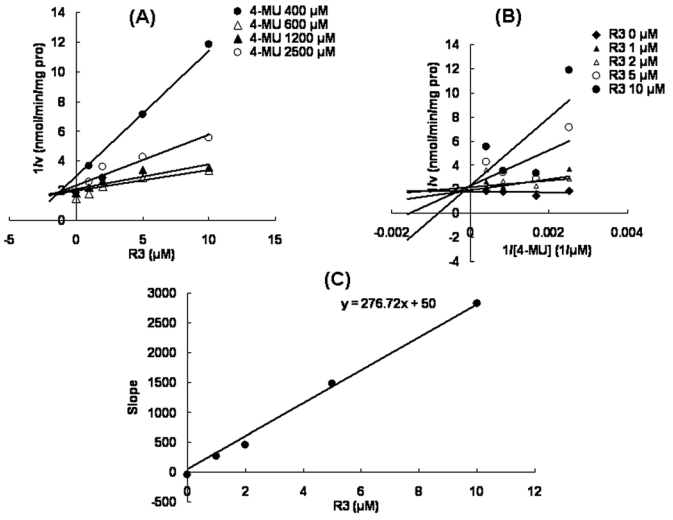

Fig. 6. Inhibition kinetics of R3 towards the activity of UGT1A3. (A) Dixon plot for the inhibition of R3 towards the activity of UGT1A3; (B) Lineweaver-Burk plot for the inhibition of R3 towards the activity of UGT1A3; (C) Second plot for the inhibition of R3 towards the activity of UGT1A3. The plot was drawn using the slopes of the lines from Lineweaver-Burk plot towards the concentration of R3.

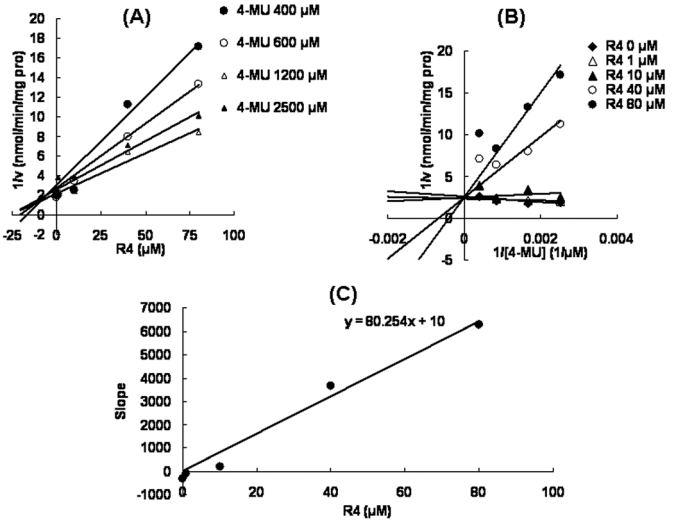

Fig. 7. Inhibition kinetics of R4 towards the activity of UGT1A3. (A) Dixon plot for the inhibition of R4 towards the activity of UGT1A3; (B) Lineweaver-Burk plot for the inhibition of R4 towards the activity of UGT1A3; (C) Second plot for the inhibition of R4 towards the activity of UGT1A3. The plot was drawn using the slopes of the lines from Lineweaver-Burk plot towards the concentration of R4.

catalyzed 4-MU glucuronidation. As shown in Figures 6A, 7A, the intersection point was located in the second quadrant in the Dixon plot. The intersection point in Lineweaver-Burk plot was located in the vertical axis (Figs. 6B, 7B). The second plot was drawn using the slopes from the Lineweaver-Burk plot towards the concentrations of R3 or R4. As shown in Figures 6C, 7C, the fitting equation was y=276.7x+50 and y=80.3x+10 for the inhibition of R3 and R4 towards UGT1A3-catalyzed 4-MU glucuronidation. Using the equations, the inhibition kinetic parameters (K_i) were calculated to be 0.2 and 0.1 μM for the inhibition of R3 and R4 towards UGT1A3, respectively.

DISCUSSION

UGTs play an important biochemical function through catalyzing the metabolism of a remarkable number of structurally diverse, endogenous, and exogenous substrates, such as bilirubin, steroids, fatty acids, and bile acids.[16] Additionally, these compounds can also inhibit the activity of UGTs. For example, endogenous substances like bile acids have been reported to exert strong inhibition potential towards several UGT isoforms. Among them, taurolithocholic acid (TLCA) exhibited the strongest inhibition towards UGT isoforms.[15] The lipid components phosphatidylcholine (PC) and lysophosphatidylcholines (LPC) showed strong inhibition towards UGT isoforms.[17] Some drugs also exhibited inhibitory behavior on the activity of UGT isoforms. For example, the antiviral drug arbidol showed strong inhibition towards the activity of UGT1A9 and UGT2B7.[18] The antidiabetes drug glimepiride exhibited strong inhibition towards UGT1A6.[19] The herbal ingredient andrographolide exhibited highly specific inhibition towards UGT2B7.[15] The inhibition of UGTs' activity by all these compounds strongly results in the disrupted metabolism of endogenous and exogenous substances.

In this study, the inhibition of UGTs' activity by rivaroxaban derivatives was investigated to indicate the possible drug–drug interaction or disrupted metabolic disorders of endogenous substances. Rivaroxaban derivatives showed the most significant influence towards UGT1A3. UGT1A3 is an important UGT isoform involved in the metabolism of estrogen and bile acids.[20,21] Recently, an experiment performed by Wang et al. showed that human UGT1A3 can conjugate 25-hydroxyvitamin D3, which is an important metabolite of vitamin D3.[22] Therefore, rivaroxaban derivatives might disrupt the metabolism of these endogenous substances. Additionally, UGT1A3 is also involved in the metabolism of some clinical drugs (e.g., nonsteroidal antiinflammatory drugs, etc.). Therefore, potential drug–drug interactions might exist between rivaroxaban derivatives and UGT1A3's substrates.

Molecular docking was used to understand the interaction between rivaroxaban derivatives and UGT1A3. We found that the alteration of chirality significantly changed the inhibition potential towards the activity cavities of UGT1A3, as indicated by computational modeling. In silico, the alteration of chirality for ligand S1 made the binding ability weaken according to the binding free energy between inhibitor and enzyme, which may be associated with the changes of hydrogen bonds and hydrophobic interactions between inhibitor and UGT1A3 enzyme. The hydrogen bonds analysis show that ligand S1 made seven hydrogen bonds to the enzyme, which is significantly higher than S2, S3, S4. Some of the hydrogen bonds in UGT1A3-S1 were formed by the interaction between S2, S3, S4, and UGT1A3; however, ligand S1 made more hydrogen bonds to residue Ser376 and His377 in the enzyme, which implies the two residues may influence the binding activity of UGT1A3-S1. Ligands R1, R2, R3, and R4 formed analogous hydrogen bonds with the UGT1A3 enzyme; all of them formed hydrogen bonds with residues Ser310 and Gln358, which may play an important role in binding of (R)-type rivaroxaban derivatives into the active pocket of the UGT1A3 enzyme. For the hydrophobic interaction, no specific residues play an important role.

However, the hydrophobic residues Leu117, Trp355, and Phe395 make contacts to ligand S1, which may contribute to the stronger binding activity of UGT1A3-S1.

In conclusion, the significant influence of rivaroxaban derivatives towards UGT1A3's activity was demonstrated in the present study. The chirality centers highly affected the inhibition behavior of rivaroxaban derivatives towards UGT1A3.

ACKNOWLEDGMENTS

This work was supported by the National Natural Science Foundation of China (No. 81202586, 81202587, 81202588), the Scientific Research Foundation for the Returned Overseas Chinese Scholars, State Education Ministry, Tianjin Project of Thousand Youth Talents, Tianjin city funded international projects to culture selected outstanding postdoctoral, and Shandong Natural Science Foundation of China (No. 2013BSE27023 and ZR2010HL023).

CONFLICT OF INTEREST

The authors declare no conflicts of interests.

LITERATURE CITED

1. Depasse F, Busson J, Mnich J. Effect of BAY 59-7939—a novel, oral, direct factor Xa inhibitor—on clot-bound factor Xa activity *in vitro*. J Thromb Haemost 2005;3:P1104.
2. Roehrig S, Straub A, Pohlmann J. Discovery of the novel antithrombotic agent 5-chloro-N-({(5S)-2-oxo-3- [4-(3-oxomorpholin-4-yl)phenyl]-1,3-oxazolidin-5-yl} methyl) thiophene- 2-carboxamide (BAY 59-7939): an oral, direct factor Xa inhibitor. J Med Chem 2005;48:5900–5908.
3. Weinz C, Schwarz T, Kubitza D. Metabolism and excretion of rivaroxaban, an oral, direct factor Xa inhibitor, in rats, dogs, and humans. Drug Metab Dispos 2009;37:1056–1064.
4. Mueck W, Kubitza D, Becka M. Co-administration of rivaroxaban with drugs that share its elimination pathways: pharmacokinetic effects in healthy subjects. Br J Clin Pharmacol 2013;76:455–466.
5. Fang ZZ, Cao YF, Hu CM, Hong M, Sun XY, Ge GB, Liu Y, Zhang YY, Yang L, Sun HZ. Structure-inhibition relationship of ginsenosides towards UDP-glucuronosyltransferases (UGTs). Toxicol Appl Pharmacol 2013;267:149–154.
6. Rowland A, Miners JO, Mackenzie PI. The UDP-glucuronosyltransferases: their role in drug metabolism and detoxification. Int J Biochem Cell Biol 2013;45:1121–1132.
7. Chen S, Yueh MF, Bigo C, Barbier O, Wang K, Karin M, Nguyen N, Tukey RH. Intestinal glucuronidation protects against chemotherapy-induced toxicity by irinotecan (CPT-11). Proc Natl Acad Sci U S A 2013;110:19143–19148.
8. Yu J, Han JC, Gao YJ. Biotransformation of glucoaurantio-obtusin towards aurantio-obtusin increases the toxicity of irinotecan through increased inhibition towards SN-38 glucuronidation. Phytother Res 2014;28:1577–1580.
9. Wei J, Ye X, Liu T. Toxicity magnification of irinotecan's toxicity by levothyroxine through inhibition of SN-38 glucuronidation. Lat Am J Pharm 2014;33:1385–1388.
10. Wang H, Fang ZZ, Zheng Y, Zhou K, Hu C, Krausz KW, Sun D, Idle JR, Gonzalez FJ. Metabolic profiling of praziquantel enantiomers. Biochem Pharmacol 2014;90:166–178.
11. Zucker SD, Qin X, Rouster SD, Yu F, Green RM, Keshavan P, Feinberg J, Sherman KE. Mechanism of indinavir-induced hyperbilirubinemia. Proc Natl Acad Sci U S A 2001;98:12671–12676.
12. Liu M, Zhang D, Yang M, Zhao T, Wang X, Zhang Y, Han J, Liu H. Pharmacokinetics of terazosin enantiomers in healthy Chinese male subjects. Chirality 2012;24:1047–1050.
13. Sun SY, Wang YQ, Li LP, Wang L, Zeng S, Zhou H, Jiang HD. Stereoselective interaction between tetrahydropalmatine enantiomers and CYP enzymes in human liver microsomes. Chirality 2013;25:43–47.
14. Fang ZZ, Wang H, Cao YF, Sun DX, Wang LX, Hong M, Huang T, Chen JX, Zeng J. Enantioselective inhibition of carprofen towards UDP- glucuronosyltransferase (UGT) 2B7. Chirality 2015;27:189–193.
15. Fang ZZ, He RR, Cao YF, Tanaka N, Jiang C, Krausz KW, Qi Y, Dong PP, Ai CZ, Sun XY, Hong M, Ge GB, Gonzalez FJ, Ma XC, Sun HZ. A model of in vitro UDP-glucuronosyltransferase inhibition by bile acids predicts possible metabolic disorders. J Lipid Res 2013;54:3334–3344.
16. Radominska-Pandya A, Bratton SM, Redinbo MR, Miley MJ. The crystal structure of human UDP-glucuronosyltransferase 2B7 C-terminal end is the first mammalian UGT target to be revealed: the significance for human UGTs from both the 1A and 2B families. Drug Metab Rev 2010;42:133–144.
17. Gao X, Qu H, Ai CZ, Cao YF, Huang T, Chen JX, Zeng J, Sun XY, Hong M, Gonzalez FJ, Liu Z, Fang ZZ. Regulation profile of phosphatidylcholines (PCs) and lysophosphatidylcholines (LPCs) components towards UDP-glucuronosyltransferases (UGTs) isoforms. Xenobiotica 2015;45:197–206.
18. Liu X, Huang T, Chen JX, Zeng J, Fan XR, Xu-Zhu YZW, Sun XY, Hong M, Sun HZ. Arbidol exhibits strong inhibition towards UDP-glucuronosyltransferase (UGT) 1A9 and 2B7. Pharmazie 2013;68:945–950.
19. Fu JF, Ren QY, Zhang NY, Gao B, Tu YY, Fu GQ, Li DH, Zhang YS. Inhibition potential of glimepiride (gli) towards important UDP-glucuronosyltransferase (UGT) isoforms in human liver. Pharmazie 2012;67:715–717.
20. Lankisch TO, Gillman TC, Erichsen TJ, Ehmer U, Kalthoff S, Freiberg N, Munzel PA, Manns MP, Strassburg CP. Aryl hydrocarbon receptor-mediated regulation of the human estrogen and bile acid UDP-glucuronosyltransferase 1A3 gene. Arch Toxicol 2008;82:573–582.
21. Erichsen TJ, Aehlen A, Ehmer U, Kalthoff S, Manns MP, Strassburg CP. Regulation of the human bile acid UDP-glucuronosyltransferase 1A3 by the farnesoid X receptor and bile acids. J Hepatol 2010;52:570–578.
22. Wang Z, Wong T, Hashizume T, Dickmann LZ, Scian M, Koszewski NJ, Goff JP, Horst RL, Chaudhry AS, Schuetz EG, Thummel KE. Human UGT1A4 and UGT1A3 conjugate 25-hydroxyvitamin D3: metabolite structure, kinetics, inducibility, and interindividual variability. Endocrinology 2014;155:2052–2063.